JACS
JOURNAL OF THE AMERICAN CHEMICAL SOCIETY

ARTICLE

pubs.acs.org/JACS

Continuous Synthesis Process of Hexagonal Nanoplates of *P6m* Ordered Mesoporous Silica

Jasper Jammaer, Titus S. van Erp, Alexander Aerts, Christine E. A. Kirschhock, and Johan A. Martens*

Center for Surface Chemistry and Catalysis, Catholic University of Leuven, Kasteelpark Arenberg 23, B-3001 Leuven, Belgium

Supporting Information

ABSTRACT: Hexagonally ordered mesoporous silica coined COK-12 was synthesized in a continuous process by combining streams of sodium silicate and citric acid/sodium citrate buffered solution of $(\text{ethylene oxide})_{20}-(\text{propylene oxide})_{70}-(\text{ethylene oxide})_{20}$ triblock copolymer (Pluronic P123) from separate reservoirs. COK-12 precipitated spontaneously upon combining both streams at nearly neutral pH and ambient temperature. Stable intermediates of the COK-12 formation process could be prepared by limiting sodium silicate addition. Investigation of these intermediates using small-angle X-ray scattering revealed COK-12 formed via an assembly process departing from spherical uncharged core−shell P123-silica micelles. The sterical stabilization of these micelles decreased upon accumulation of silicate oligomers in their shell. Aggregation of the spherical micelles led to cylindrical micelles, which aligned and adopted the final hexagonal organization. This unprecedentedly fast formation of *P6m* ordered mesoporous silica was caused by two factors in the synthesis medium: the neutral pH favoring uncharged silicate oligomers and the high salt concentration promoting hydrophobic interactions with surfactant micelles leading to silica accumulation in the PEO shell. The easy continuous synthesis process is convenient for large-scale production. The platelet particle morphology with short and identical internal channels will be advantageous for many applications such as pore replication, nanotube or fiber growth, catalytic functionalization, drug delivery, film and sensor development, and in nano dyes as well as for investigation of pore diffusion phenomena.

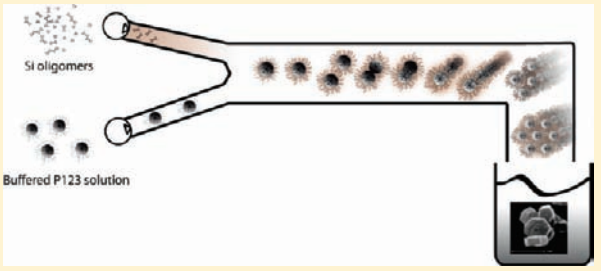

INTRODUCTION

Ordered mesoporous silica materials are finding their way into applications in drug delivery, molecular separation, catalysis, and sensor and optical devices.[1−7] Since their introduction in 1992, especially materials with *P6m* symmetry with hexagonal arrangement of parallel channels have inspired the research community.[8,9] While the popular MCM-41 is synthesized under basic conditions with quaternary alkyl ammonium surfactants, SBA-15 typically is obtained under strongly acidic conditions in the presence of Pluronic P123 triblock copolymer ($(\text{ethylene oxide})_{20}-(\text{propylene oxide})_{70}-(\text{ethylene oxide})_{20}$).[8−11] Some simplifications of the original synthesis procedure such as the use of sodium silicate instead of silicon alkoxides have been reported.[12−15] The supramolecular chemistry of the formation of ordered mesoporous silica materials is presently explained in terms of formation and assembly of silica-covered surfactant micelles.[9,10,16−24] It has been argued that at high and low pH, for MCM-41 and SBA-15 preparation respectively, the coassembly of surfactant molecules and silicate species proceeds through charge density matching mechanisms.[10,25] The need for strongly acidic or basic pH synthesis conditions has been disproven by successful syntheses of MSU-H involving neutralization of the acidic surfactant solution by the alkaline solution of sodium silicate.[26,27] Earlier, we demonstrated feasibility of a buffered P123 surfactant solution at pH 5−6 as synthesis medium.[28,29] Addition of sodium silicate solution to citrate/citric acid buffered triblock copolymer solution at room temperature led to spontaneous precipitation of *P6m* ordered mesoporous material, coined COK-12.[28,29]

The field of ordered mesoporous materials faces severe scientific and technological challenges. While continuous synthesis processes of zeolites have been conceived, to our knowledge there are no reports on continuous synthesis protocols for ordered mesoporous materials.[30,31] Very high levels of local mesoscopic ordering easily can be obtained in the current ordered mesoporous silica materials, but control over continuity and straightness of mesopores is not always obvious. Nanoplates with short straight channels are of interest for diffusion and adsorption studies,[32,33] pore replication and nanocasting,[34] mesoporous film deposition, and templated nanotube growth[35,36] and allow deposition of catalytically active elements.[37] But synthesis of the desired uniform, ultrathin, and mesoporous nanoplates is difficult. Chen et al. added zirconium to the synthesis mixture and used prehydrolyzed TEOS for preferential growth of hexagonal platelets with a thickness of 200−350 nm.[33] Linton et al. identified a point in time during synthesis of SBA-15 where a manipulation, such as salt addition, altered the particle morphology and provoked preferential platelet growth.[21,33,38] Recently, Lee et al. investigated the development of SBA-15

Received: June 17, 2011
Published: July 26, 2011

particle morphology in great detail: conditions usually favoring 1 μm long hexagonal rods with mesopores in longitudinal direction led to shortened morphology (450 nm) upon tuning the EO portion of EO−PO−EO triblock copolymer.[39]

Here we report a continuous synthesis process of *P6m* ordered mesoporous silica platelets with short channels crossing a uniform plate thickness of ca. 250 nm. The observation of stable synthesis intermediates upon limited silicate addition and their ex situ investigation with SAXS revealed the steps of the supramolecular formation mechanism and explained why COK-12 material was formed that easily.

METHODS AND MATERIALS

Continuous COK-12 Synthesis. Buffered P123 solutions and diluted sodium silicate solutions were prepared in polypropylene beakers. A typical P123 surfactant solution, buffered at pH 5, was prepared by dissolving P123 surfactant (111.8 g, BASF, Belgium) in demineralized water (2928 g) before citric acid (100.2 g, monohydrate, Sigma Aldrich) and trisodium citrate (69.1 g, dihydrate, Sigma Aldrich) were added. The P123 solution was stirred overnight at room temperature with a magnetic stirring bar (300 rpm). A standard sodium silicate solution was prepared from commercial sodium silicate solution (145.3 g, 27% SiO_2, 10% NaOH, extra pure, Merck) by dilution with 419.7 g of demineralized water.

One syringe (Braun, 50 mL) was filled with buffered P123 surfactant solution and another one with silicate solution. The syringes were mounted in B. Braun's Perfusor Space Syringe Pumps. Both pumps were started simultaneously. The flow rate was 198 and 70 mL/h for the surfactant and silicate solution, respectively. Liquids were jetted through Teflon tubing (20 cm long, i.d. 1.6 mm) and combined in a Swagelok T piece connected to an outflow tubing (30 cm long, i.d. 3.2 mm). The product slurry was recovered, vacuum filtrated, and washed with demineralized water. The solid product was dried at 60 °C overnight and part of it calcined in an oven at 350 °C for 6 h using a 1 °C/min heating ramp.

In a larger scale continuous synthesis setup, surfactant and sodium silicate solution were fed from their respective reservoirs using hose pumps. The surfactant solution was pumped by a Cole Palmer Masterflex I/P Precision Brushless Drive, with I/P Easy-Load pump head making use of Masterflex Tygon Chemical Tubing I/P 26 (i.d. 6.4 mm). The silicate solution was pumped by a Cole Palmer Masterflex L/S precision variable-speed drive with L/S High-Performance Pump Head making use of Masterflex Tygon Chemical Tubing, L/S15, i.d. 4.8 mm. The surfactant solution pump rotor speed was set at 29 (scale 5−100) which corresponded to ca. 1130 mL/min. The silicate solution pump rotor analogue controller was set to level 6 which corresponded to ca. 420 mL/min. Pumps were started at the same time. The two liquid streams were combined in a glass Y piece (i.d. inlet tubing for surfactant: 4 mm; i.d. tubing for inlet sodium silicate solution: 3 mm, i.d. the outlet: 4 mm) and collected through an 180 cm long outlet tube (Masterflex, Tygon Chemical, I/P 26, i.d. 6.4 mm). During the first 10 s the product was not retained. Subsequently the product was collected for 4 min in a glass beaker. Ten minutes after collection the slurry was vacuum filtrated and washed with demineralized water. The sample was air-dried at 60 °C.

For the investigation of the synthesis process with SAXS, 2 g of buffered surfactant solution was introduced in a flask. Quantities of 0.050, 0.100, 0.200, 0.250, 0.300, 0.350, 0.400, 0.500, and 0.670 mL of sodium silicate stock solution were added using a micropipet while stirring. This corresponded to 7.5, 15, 30, 37.5, 45, 52.5, 60, 75, and 100% of the nominal silicate amount used in a typical synthesis of COK-12.

Characterization Techniques. Dynamic light scattering was performed on a Brookhaven 90Plus Particle Size Analyzer instrument. Particle size distributions were obtained by processing the correlation functions with the Clementine package for modeling of decay kinetics based on Maximum Entropy method in Igor Pro 6.02A.[40] The correlation functions were also processed with the cumulant method for comparison.[41]

SAXS patterns of powder samples were recorded at room temperature by using a SAXSess mc^2 instrument (Anton Paar, Graz, Austria) with line-collimated CuKα radiation and a 2D imaging plate detector. SAXS patterns were normalized to incident beam intensity. Background subtraction (empty capillary) and correction for instrumental broadening were performed by using the SAXSquant software. In the study of the formation mechanism, the synthesis mixtures were injected in a stop flow cell mounted in the SAXSess mc^2 instrument. The temperature was controlled using a Peltier device and kept constant at 25 °C. The buffer solution was measured as a background. The recorded SAXS patterns were fitted with a model based on work by Sundblom et al.[24,42] This model is a core shell cylinder model that also accounts for stacking of the cylinders in ordered structures. The theoretical basis is summarized in the Supporting Information.

Nitrogen adsorption isotherms were recorded at −196.8 °C on a Micromeritics Tristar 3000 apparatus after degassing the calcined powder samples at 200 °C for 10 h under nitrogen flow. Micropore volumes were estimated using the Alpha S method. BET surface areas were estimated in the P/P° region 0.05−0.3. Transmission electron microscopy (TEM) was performed on an Philips FEG CM200 operating at 200 kV. Samples were prepared on 50 nm 300-mesh carbon-coated copper grids. SEM images were obtained on an SEM Philips XL 30 FEG apparatus. Samples were spread on carbon tape and coated with gold. The ^{29}Si MAS NMR spectra were recorded on a Bruker AMX300 spectrometer operating at 100 MHz. Four thousand scans were accumulated with a recycle delay of 60 s. The samples were packed in 4 mm zirconia rotors. The spinning frequency of the rotor was 5000 Hz. Tetramethylsilane was the chemical shift reference.

RESULTS AND DISCUSSION

In previous work we reported the spontaneous formation of COK-12 ordered mesoporous silica upon combining solutions of sodium silicate and Pluronic P123 triblock copolymer surfactant in the presence of citric acid/citrate buffer.[28,29] Here we explored synthesis of COK-12 in a continuous process. In a first experiment buffered triblock copolymer solution and sodium silicate solution were separately fed using perfusion pumps. The two streams were fed from separate reservoirs by tubing and combined in a T-connection provided with an outlet tube. Immediate precipitation was observed in the beaker in which the product was collected. According to SAXS the precipitate was COK-12. In this setup with perfusion pumps ca. 0.075 g of COK-12 was produced per minute. In a larger scale setup using hose pumps feeding the buffered P123 and sodium silicate solution, respectively, a production rate of 30 g/min of COK-12 was achieved. The product was filtered, dried at 60 °C, and calcined at 350 °C to evacuate the surfactant from the pores. Experimental details and product properties of continuously produced COK-12 are listed in Table 1.

Very thin platelets of uniform thickness of ca. 250 nm were obtained (Figure 1).

The continuously synthesized COK-12 product was highly ordered as evidenced by SAXS (Figure 2A). All diffractions could be indexed in the *P6m* space group. Higher order (21), (30), (22), (31) reflections were detected indicating the excellent

Table 1. Continuous Synthesis Conditions and Product Properties of COK-12

sample setup	flow rate A[a] (mL/min)	flow rate B[a] (mL/min)	COK-12 yield (g/min)	d_{10}[b] (nm)	d_p[c] (nm)	W[d] (nm)	BET[e] (m^2/g)	$V_{\mu p}$[f] ($cm^3\ g^{-1}$)	V_p[g] (cm^3/g)
1 Perfusor syringes	3.3	1.16	0.075	8.89	6.1	4.20	663	0.15	0.62
2 hose pumps	1130	420	30	8.92	5.9	4.45	600	0.08	0.61

[a] A = Buffered triblock copolymer solution; B = Sodium silicate solution. [b] Hexagonal unit cell parameter. [c] Mesopore diameter. [d] Wall thickness. [e] BET specific surface area. [f] Micropore volume . [g] Cumulative pore volume.

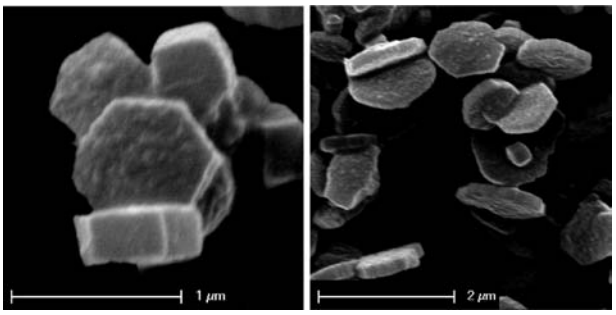

Figure 1. SEM micrographs of calcined sample 2.

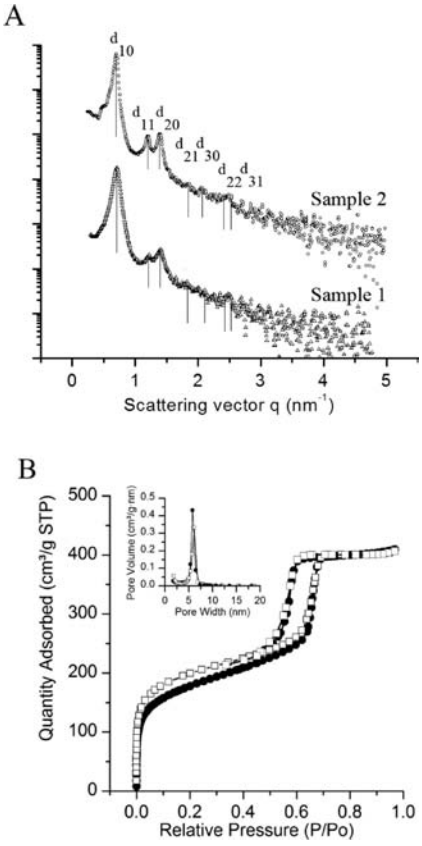

Figure 2. (A) Small angle X-ray scattering patterns of calcined samples 1 and 2. (B) Nitrogen adsorption isotherms of sample 1 (squares) and sample 2 (circles) prepared in continuous synthesis process. The BJH pore size distributions are shown in the inset.

ordering. Nitrogen adsorption isotherms (Figure 2B) for both samples calcined at 350 °C displayed H1 hysteresis loops with steep branches, typical of mesoporous materials with one type of

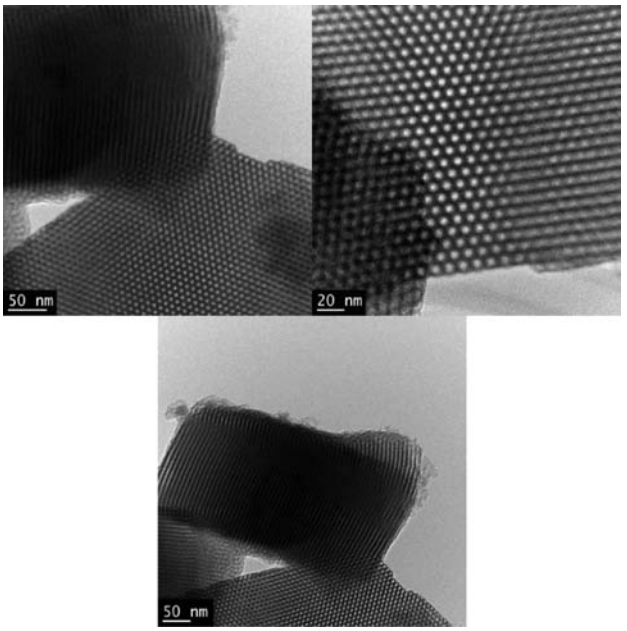

Figure 3. TEM micrographs of sample 2 (calcined).

mesopores. The pore size distribution was narrow, with a mean pore diameter of 6.1 ± 0.4 and 5.9 ± 0.3 nm in samples 1 and 2, respectively (Table 1). The BET surface area of the materials was approximately 600 $m^2\ g^{-1}$. ^{29}Si MAS NMR spectra (Supporting Information) of as-synthesized materials showed three signals at ca. 92, 101, and 110 ppm, assigned to Q_2, Q_3, and Q_4, respectively, with intensity distributions of 7.5%, 42.1%, and 50.4%, respectively, for sample 1 and 9.7%, 45.5%, and 44.8%, respectively, for sample 2. Q_n stands for a silicon atom with n siloxane bridges and 4 - n hydroxyl groups. TEM micrographs (Figure 3) viewing along and parallel to the channels of calcined sample 2 confirmed platelet morphology with channels parallel to the short axis and excellent ordering throughout individual platelets.

Intrigued by the ease of synthesis and high quality of the COK-12 material, the formation process of this material was investigated. In diluted aqueous solution P123 triblock copolymer forms spherical micelles composed of a rather dense core of polypropylene (PPO) oxide moieties and a diffuse shell of poly(ethylene oxide) (PEO) chains.[43] The extending PEO chains are responsible for steric stabilization of the micelles.[43] Sphere to rod transition of P123 micelles is known to occur in the presence of salt at high concentration.[44−47] The effect of salt ions relates to their water structuring capacity, which directly affects the hydrophobic effect and therewith the solubility of organic species in water. According to the Hofmeister series, which describes this phenomenon, citrate is particularly suited to

enhance hydrophobic interaction between the triblock copolymer chains:[48]

$$\text{citrate}^{3-} > \text{sulfate}^{2-} > \text{phosphate}^{2-} > F^- > Cl^-$$

The aggregation state of P123 surfactant in the buffered solution was determined using dynamic light scattering (DLS) at varying times (Supporting Information). Different models were used to estimate the size of the micelles. Analysis via the cumulant method returned micelle sizes of 20 nm, slightly larger than in the absence of citric acid/citrate buffer where micelles measured 18 nm. These values are in agreement with those reported in the literature.[47] Hydrodynamic diameters of ca. 15 and 14 nm were obtained by applying the maximum entropy model for the buffered and the reference P123 solution, respectively.[40,49] The observation of spherical micelles in the buffered P123 sample showed that the citrate did not induce micellar growth in our system, not even after several weeks.

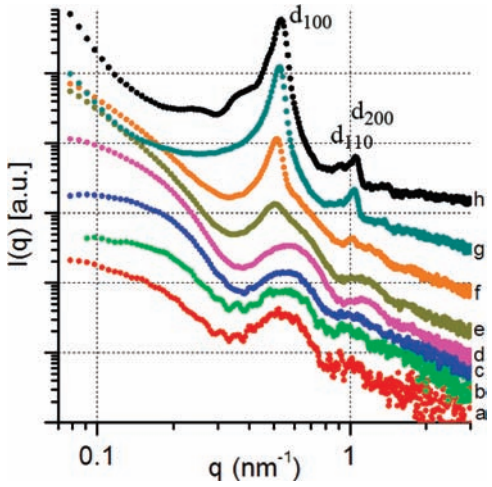

Figure 4. SAXS patterns of buffered P123 triblock copolymer solutions with increasing percentages of the nominal amount of sodium silicate: a, 7.5%Si; b, 15%Si; c, 30%Si; d, 45%Si; e, 52%Si; f, 60%Si; g, 75%Si, and h, 100%Si, corresponding to a standard synthesis. Curves were shifted vertically for clarity.

A series of samples of buffered P123 solutions to which only a percentage of the nominal sodium silicate amount was added (denoted as "%Si ") were prepared. The samples were studied by small-angle X-ray scattering measurements. While the intensity of the SAXS pattern of the buffered P123 solution was weak and unresolved due to the low scattering contrast between organic micelles and solvent, the SAXS pattern intensity increased after sodium silicate addition (Figure 4). A representative series of SAXS patterns with increasing silica concentration is shown in Figure 4. Repeated measurement of the samples after 24 h confirmed stability over at least 1 day.

Samples with Si contents below 45% displayed only broad scattering signals (spectra a−d in Figure 4). Emerging Bragg scattering was observed from sample 52%Si onward (spectra e−h in Figure 4). A variety of models were evaluated for fitting of these SAXS patterns, including hard spheres, hard cylinders, core−shell spheres and cylinders, and polydisperse core−shell spheres and cylinders.[50] The SAXS patterns of all samples in the range 7.5−100%Si were successfully fitted using a simplified version of the core−shell cylinder model by Sundblom et al. that includes description of the crystallization of the cylinders into hexagonal lattices.[24] Representative SAXS patterns and corresponding fits are shown in Figure 5. Application of the full model by Sundblom et al. was not attempted as it involves a significant number of additional fitting parameters and its solution does not provide further information on the length of the

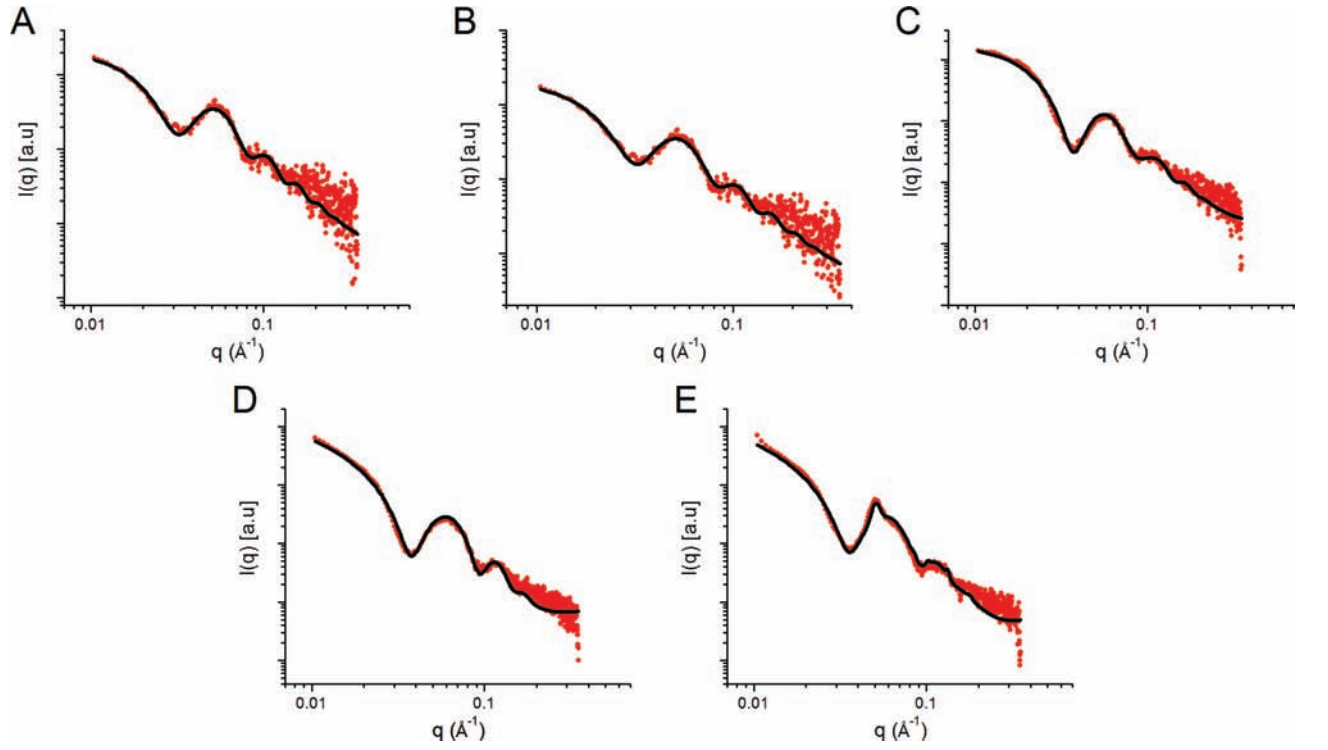

Figure 5. SAXS patterns and corresponding fits of surfactant solutions to which 7.5% (A), 15% (B), 30% (C), 45% (D), and 52% (E) of the nominal silica content was added. All patterns were fitted with a simplified Sundblom et al. model for core shell cylinders (Supporting Information).

Table 2. Dimensions of Coated Micelles Estimated from Fitting of SAXS Patterns of P123 Surfactant Solutions to Which a Percentage of the Silica Content of a Standard Synthesis Was Added

	polydisperse core/shell cylinder Sundblom (simplified)			polydisperse core−shell sphere
%Si	L (nm)	d cylinders (nm)	T (nm)	d spheres (nm)
7.5				14.8
	11.0	11.5	0.8	
15				14.0
	11.4	10.0	0.9	
30	12.7	10.7	1.4	
37.5 ([a])	39.4[a]	11.7[a]	1.4[a]	
45 ([a])	>90; (91.9[a])	9.2; (11.9[a])	2.3; 2.2[a]	
52	250[b]	9.6	2.0	
60	250[b]	10.7	2.2	

[a] Additional low q SAXS patterns were recorded for improved determination of the cylinder length (Supporting Information). [b] L = fixed.

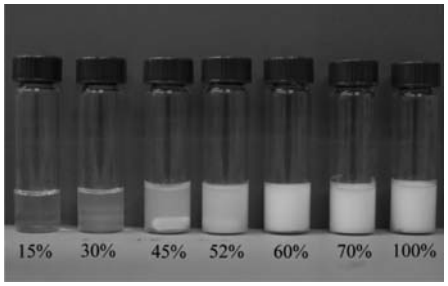

Figure 6. Photographs of samples prepared in the formation study of COK-12 material, with increasing amount of the nominal Si content (rel. to standard synthesis). From left to right: 15%Si, 30%Si; 45%Si; 52%Si; 60%Si; 75%Si; 100%Si.

cylinders.[24,42] Micelle−silica composite dimensions are listed in Table 2.

Fitting of the SAXS patterns of 7.5%Si and 15%Si samples with the cylindrical model gave rise to similar values for the cylinder length and the diameter, approximately 11 nm (Table 1), identifying the spherical shape of the core−shell micelles. A shell thickness of 0.8−0.9 nm was derived as a fitting parameter yielding total dimensions of approximately 13 nm. Additional modeling of the 7.5%Si and 15%Si patterns with a polydisperse spherical core−shell model confirmed the spherical shape (Supporting Information).[50] Total diameters of the spheres were estimated at ca. 14.8 nm at 7.5%Si and ca. 14.0 nm at 15%Si (Table 2). These dimensions of the coated micelles were consistent with those of the original P123 micelles of around 14 nm determined with DLS (vide supra) and the values reported in literature. SANS measurements by Zhobolenko et al. of a typical SBA-15 surfactant mixture based on P123 revealed a core diameter of spherical micelles of 8.2 nm and a total diameter of 14.2 nm.[23] Based on an experimentally determined average aggregation number of 86 in a similar, diluted solution Zhou et al. estimated the core to have a theoretical diameter of ca. 10.4 nm.[51]

The excellent fitting of SAXS patterns at 7.5%Si and 15%Si (Figure 5A) and the almost unaltered size after silicate addition suggested silica to be concentrated in the PEO-rich outer shell of the spherical micelles, in interaction with PEO chains, and without increasing the size of the original micelles. While the form factors of the 7.5%Si and 15%Si samples were identical (spectra a and b in Figure 4), the SAXS signal intensity of the 15% Si sample was approximately 1.5 times stronger than at 7.5%Si revealing a systematic increase of the silica content in the shell of individual micelles. When more than 15%Si was added the SAXS pattern was changed (spectra c, d in Figure 4). The shell of the micellar−silicate composites grew, attaining 1.4 nm at 30%Si, and the composites tended to adapt a cylindrical shape, as was confirmed by the growth in length derived from the modeling of the SAXS patterns. The length increase in the 30%Si sample was minor, but upon further addition of Si the cylinders drastically lengthened. Additional, very low q_{min}, SAXS patterns (0.04 nm^{-1}, Supporting Information) were recorded to improve accuracy of the length determination of the cylinders. Lengths increased to ca. 40 nm at 37.5%Si (Supporting Information) and already exceeded 90 nm at 45%Si (Table 2, Supporting Information). The growth in length occurs evenly for all cylinders as can be concluded from the low length polydispersity 90 ±10 nm (Supporting Information). Throughout the growth in length, the core diameter of the cylinders remained nearly constant and the shell was approximately 2 nm thick.

Table 3. Unit Cell Parameter a of the Samples Prepared by Addition of Silicate Precursor in Different Amounts

%Si	a (nm)
52	14.4
60	14.2
75	13.9
100	13.7

The growth of the micellar silica composites was in agreement with the visual macroscopic appearance of the samples (see Figure 6). Samples with 7.5%Si, 15%Si, and 30%Si were clear solutions, as expected for suspensions of spherical or cylindrical particles with dimensions below 20 nm. The cylinder growth process in the 45%Si sample was accompanied by the transition from a viscous, opalescent sol into a gel. While the 52%Si sample was still a viscous gel, at 60%Si and higher silica contents the samples were suspensions of particles.

In the 52%Si sample the d_{100} diffraction peak, characteristic of mesoscale ordering, was superimposed on the form factor (spectrum e in Figure 4). At this stage of silica addition the cylindrical micelles started aggregating. The hexagonal symmetry of the packing was apparent from the d_{11} and d_{20} signals in SAXS patterns at 60% Si and higher (spectra f−h in Figure 4). Based on the intensity increase of the d_{10} diffraction peak upon Si added amounts, growth of fully ordered domains could be deduced (spectra f−h in Figure 4). The intensity increase was accompanied by a relatively small shift in q toward higher values. This indicated contraction of the unit cell parameter upon addition of more silicate. The unit cell parameters of the different samples are listed in Table 3. The contraction of the unit cell with increasing silicate content implied increasing density of the silicate walls.

These SAXS experiments led to the proposal of the following formation mechanism (Figure 7). In the strongly basic sodium silicate solution, silica is mostly present as two times dissociated orthosilicic acid, $SiO_2(OH)_2^{2-}$. Upon addition to the buffered P123 solution at pH 5, the silicate anions are protonated and

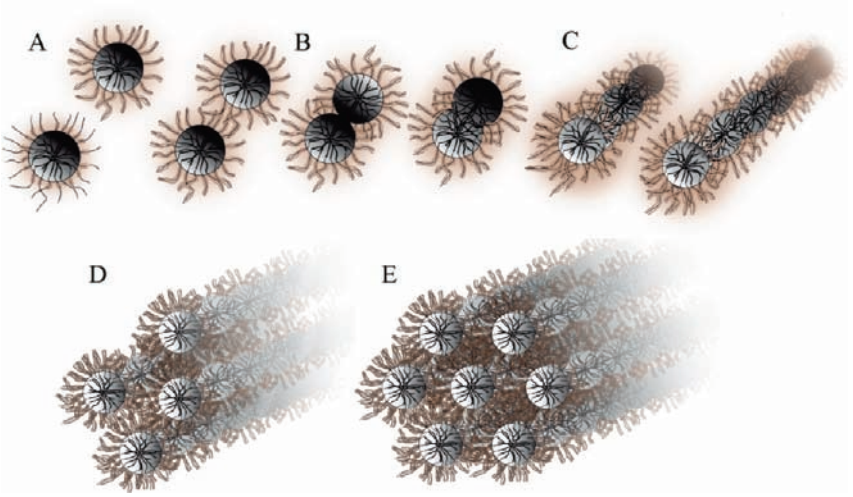

Figure 7. Schematic representation of stages in the formation of COK-12 mesoporous silica at RT and quasi-neutral pH. On the P123 micelles, silica is precipitated on the PEO blocks of the micelles protruding into the solution (A). At a critical silica addition, steric stabilization is lifted (B) and spherical micelles coalesce into cylinders which increase in size (C, D). Further addition of silica leads to aggregation of cylinders and eventually to hexagonally mesostructured material (E).

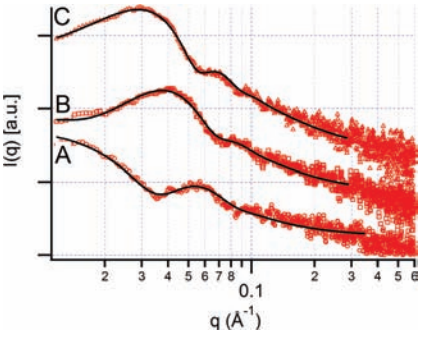

Figure 8. SAXS pattern of spherical composite surfactant−silica (approximately 15%Si, A) to which a small amount of TMB (TMB: P123 0.21 weight ratio) was added, measured immediately (B) and after 3 h (C).

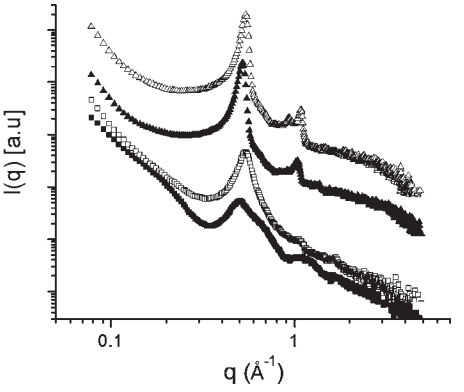

Figure 9. SAXS patterns of surfactant solutions to which 52% (squares) and 75% (triangles) of the nominal silica content was added, measured directly after preparation (filled) and after 7 days (open).

neutralized to orthosilicic acid molecules, $Si(OH)_4$, which at that pH are expected to oligomerize rapidly into small, little dissociated silicate oligomers. The interaction between silicate oligomers and poly(ethylene oxide) has been investigated by Takahasi et al. using SAXS and ^{29}Si NMR.[52] Strong attractive interaction between silicate oligomers and PEO limiting the degree of cross-linking of the silicate network was observed.[52] The sodium concentration of the buffered solution was ca. 0.1 mol/L. The sodium content of as-synthesized COK-12 material determined via dissolution and AAS was surprisingly low and below the detection limit of 1 ppm. The absence of charge compensating cations in the final, ordered mesoporous silica confirmed that the silica polymer contained very few negative charges needing charge compensation by sodium ions. The zeta potential of the core−shell P123-silica micelles was determined and indeed was close to zero. In addition to the organic−inorganic interaction, a salting out effect of the neutral silicate molecules may have assisted the enrichment of silica in the micelle shells.[53] Recently, in line with our reasoning, Teixeira et al. revealed that inorganic salt speeds up the formation of SBA-15 mesophases by influencing the P123 micellar properties rather than kinetics of silicate polymerization.[54]

With increasing silica concentration from 7.5%Si to 15%Si the size of the micelles remained almost constant (Table 1) meaning that the silica content of the diffuse PEO layer was increased (Figure 7a). Absence of a zeta potential on the micelles pointed out stabilization must have been due to steric effects of the PEO chains. Silica incorporation in the diffuse layer of PEO chains probably decreased their mobility as well as their degree of solvation. At Si additions beyond 15%Si individual spherical micelles started aggregating into cylinders. The transition from spheres to cylinders with similar diameter (Table 1) was interpreted as a coalescence process wherein PPO cores merged to form the core of a cylinder, with silica embedded in PEO constituting a mantle (Figure 7b). The proposed coalescence necessitates sufficient flexibility of the silica−PEO composite to allow merging of PPO cores. The formation of platelets with a limited and uniform thickness (Figure 1) reflects the physical limitation of the length a linear aggregate of spheres can reach.

The flexibility of the spherical P123-silica core−shell micelles was demonstrated by the following experiment. 1,3,5-Trimethylbenzene (TMB) known as a swelling agent of P123 micelles was

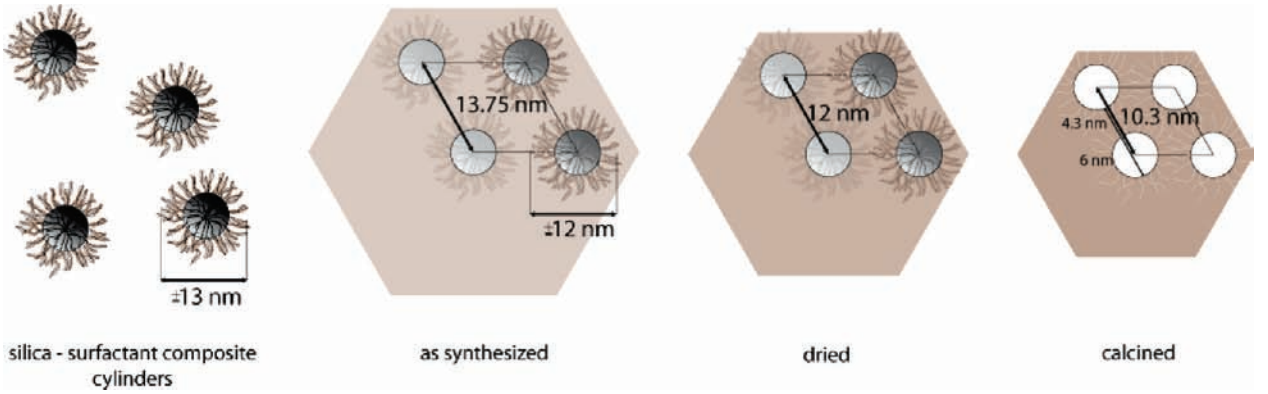

Figure 10. Micellar cylinder and unit cell size of as synthesized, dried, and calcined COK-12 material.

added to a micelle suspension with 15%Si.[11] Initially, the organic molecule was phase-separated as a liquid layer on top of the aqueous micelle suspension, but after several hours a homogeneous mixture was obtained (Figure 8c). According to SAXS the micelles steadily expanded from 12.2 to 19.4 nm (Figure 8, Supporting Information). The observed swelling capacity revealed the presence of an expandable silicate network with a limited degree of cross-linking to enable the swelling, in agreement with earlier work.[43]

Upon further addition of silica, the cylinders grew longer until they started aggregating into a hexagonal pattern. The development of ordered material proceeded faster with increasing silicate content. According to SAXS in samples with 52%Si the crystallization took several days. SAXS patterns of 52%Si and 75%Si samples measured immediately after preparation and after 1 week are shown in Figure 9. The slow growth of ordered domains in the 52%Si sample evidenced that, when a critical coating and micelle length is achieved, ordering eventually can occur. In samples with higher Si content the hexagonal ordering of the cylindrical micelles was much faster, seconds to minutes in the case of 100%Si. Obviously, increasing silica addition eliminated the steric stabilization of the cylinders.

The sequence of the events and the necessity of lifting steric stabilization to enable aggregation can explain the ease of formation and the excellent quality of the mesoscopic ordering. Micelles that are insufficiently coated with silica will, for steric reasons, not participate in the aggregation until they reach the critical silica content. It explains why the mixing conditions of buffered P123 and sodium silicate solutions are less critical, and why in a continuous synthesis process jetting together of the two components is effective to produce a highly ordered material.

The pore size of the final COK-12 material obtained at 100%Si addition was in agreement with the proposed formation process (Figure 7). The hexagonal unit cell parameter derived from the d_{10} spacing of the 100%Si sample was 13.75 nm. This diameter is close to that of the cylinders, which measure, e.g., 13.6 nm in the 52%Si sample (Table 2). Upon drying at 60 °C under air, the unit cell shrunk to 12 nm and upon calcination at 350 °C to 10.3 nm. The pore diameter of COK-12 synthesized at room temperature, estimated via nitrogen adsorption of calcined samples, invariably was 5.5−6 nm.[28,55] According to the formation process this size should correspond to the diameter of the PPO core of the original cylindrical micelles (Figure 10). Combination of the unit cell parameter and the pore size estimated a wall thickness of ca. 4 nm, which therefore should correspond to twice the shell

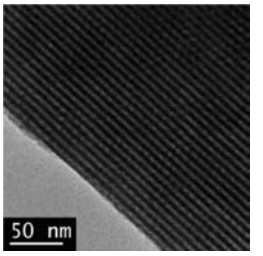

Figure 11. TEM micrograph of sample 2 revealing pore corrugation.

thickness of 2 nm.[28,29] The presence of pore corrugation revealed by TEM at a repetition of ca. 6 nm (Figure 11) can be interpreted as incomplete merging of spherical micelles into cylinders.[56]

In earlier investigations of SBA-15, synthesis cryo-TEM and in situ synchrotron SAXS were applied to gain insight in the formation mechanism.[16−19,21−24] In general, a sequence of coating of spherical polymer micelles with silica, followed by or coinciding with a transformation to silica-coated cylinders, and finally a hexagonal stacking of cylinders were observed.[16−19,21−24] For SBA-15 formation it remains unclear whether initial micelles grow by uptake of dissolved surfactant monomers or by aggregation, and whether the early precipitates require internal rearrangement to achieve order. Ruthstein et al. identified coated spherical P123-silica micelles in the early stages which transformed gradually into cylindrical micelles in coexistence with spherical species.[16,17] Bundles of cylinders were formed which led to a precipitate, initially lacking order. Internal rearrangement led to the final, ordered material. Sundblom et al. observed micelle elongation by increase of the aggregation number caused by interaction of PEO chains with silicate oligomers.[24] In the study by Zholobenko et al., ordering of the cylindrical bodies and precipitation coincided.[22,23,57] Alfredsson's team had a slightly different view and described the formation of flocs containing spherical micelles which coalesced to form cylinders.[19,21] Those investigations on SBA-15 formation mechanisms were quite involved and necessitated heating and in situ SAXS experiments. The study of the formation process of COK-12 was facilitated by the availability of stable intermediates, and the sequence of events was much more evident. Despite the use of the same P123 surfactant in COK-12 and SBA-15 synthesis, there seem to be differences in the formation process. Stucky et al. emphasized the importance of strong electrostatic interactions during SBA-15 self-assembly.[10] At a pH below the isoelectric point of silica at which

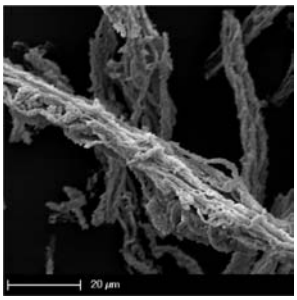

Figure 12. SEM micrographs of a sample obtained performing COK-12 synthesis in the presence of ethanol.

SBA-15 is formed, both the inorganic silica and the P123 surfactant are partially protonated. The positive charges are compensated by chlorine anions X^-, and the assembly process is indicated as $N^0H^+X^-I^+$, with N^0 standing for the nonionic surfactant and I^+ for the positively charged inorganic silica. In the synthesis of COK-12 electrostatic interactions do not play a role. The speed of the assembly of COK-12 even at room temperature can be explained by the absence of surface charges on the micelles facilitating aggregation, once the increasing presence of silica in the PEO shell had overcome steric stabilization. The rapid consumption of spherical silica-coated spherical micelles resulted in relatively short-coated cylinders with a narrow length distribution. In the absence of any charge stabilization, a fast aggregation of the coated cylinders directly led to the platelet morphology typical for COK-12.

The use of TEOS in the synthesis of an ordered mesoporous material upon hydrolysis leads to the formation of ethanol which interferes with the colloid chemistry of the P123 surfactant.[44,46,58] A synthesis experiment was performed using the standard composition for COK-12 and addition of 10 wt % ethanol to the surfactant stock solution. The obtained ordered mesoporous material had a fibrous appearance (Figure 12). Ethanol provoked the formation of elongated P123 surfactant micelles before coating with silica.

CONCLUSIONS

In conclusion, a convenient, continuous synthesis process for COK-12 hexagonal ordered mesoporous silica platelets with excellent mesopore ordering and very short pore lengths of merely 250 nm was developed. The formation mechanism of COK-12 was revealed based on the nature of stable intermediates, obtained by stepwise addition of the sodium silicate. The formation process departs from spherical P123 triblock copolymer micelles. Neutral silicate oligomers penetrate into the PEO layer and decrease steric stabilization leading to coagulation and formation of cylindrical micelles by attachment of individual spherical micelles. Lateral aggregation in a hexagonal pattern leads to formation of the final particles. The peculiar platelet morphology reflects the size of these cylindrical micelles which for stability reasons seems limited to about 250 nm.

The present material is expected to overcome problems encountered with current materials regarding particle morphology and pore imperfections. The short uniform channels of COK-12 should be ideally suited for investigating diffusion, replication, and functionalization and in development of applications critically depending on pore uniformity.

ASSOCIATED CONTENT

Supporting Information. (1) ^{29}Si MAS NMR spectra of COK-12 materials, (2) DLS measurement of uncoated micelles, (3) modeling of SAXS patterns, (4) TMB experiment swelling of coated micelles, (5) COK-12 continuous synthesis perfusion pumps, and (6) COK-12 continuous synthesis hose pumps. This material is available free of charge via the Internet at http://pubs.acs.org.

AUTHOR INFORMATION

Corresponding Author
Johan.Martens@biw.kuleuven.be

ACKNOWLEDGMENT

C.E.A.K. and J.A.M. acknowledge the Flemish government for long term structural funding (Methusalem). A.A. acknowledges FWO for a postdoctoral fellowship. The authors thank G. D. Stucky for the constructive discussion at Prepa10.

REFERENCES

(1) Hartmann, M. *Chem. Mater.* **2005**, *17*, 4577–4593.
(2) Vallet-Regí, M.; Balas, F.; Arcos, D. *Angew. Chem., Int. Ed.* **2007**, *46*, 7548–7558.
(3) Mellaerts, R.; Aerts, C. A.; Van Humbeeck, J.; Augustijns, P.; Van den Mooter, G.; Martens, J. A. *Chem. Commun.* **2007**, 1375–1377.
(4) Giraldo, L. F.; Lopez, B. L.; Perez, L.; Urrego, S.; Sierra, L.; Mesa, M. *Macromol. Symp.* **2007**, *258*, 129-141 230.
(5) Monnier, A.; Schuth, F.; Huo, Q.; Kumar, D.; Margolese, D.; Maxwell, R. S.; Stucky, G. D.; Krishnamurty, M.; Petroff, P.; Firouzi, A.; Janicke, M.; Chmelka, B. F. *Science* **1993**, *261*, 1299–1303.
(6) Scott, B. J.; Wirnsberger, G.; Stucky, G. D. *Chem. Mater.* **2001**, *13*, 3140–3150.
(7) Corma, A. *Chem. Rev.* **1997**, *97*, 2373–2419.
(8) Kresge, C. T.; Leonowicz, M. E.; Roth, W. J.; Vartuli, J. C.; Beck, J. S. *Nature* **1992**, *359*, 710–712.
(9) Beck, J. S.; Vartuli, J. C.; Roth, W. J.; Leonowicz, M. E.; Kresge, C. T.; Schmitt, K. D.; Chu, C. T. W.; Olson, D. H.; Sheppard, E. W.; McCullen, S. B.; Higgins, J. B.; Schlenker, J. L. *J. Am. Chem. Soc.* **1992**, *114*, 10834–10843.
(10) Zhao, D.; Huo, Q.; Feng, J.; Chmelka, B. F.; Stucky, G. D. *J. Am. Chem. Soc.* **1998**, *120*, 6024–6036.
(11) Zhao, D.; Feng, J.; Huo, Q.; Melosh, N.; Fredrickson, G. H.; Chmelka, B. F.; Stucky, G. D. *Science* **1998**, *279*, 548–552.
(12) Celer, E. B.; Jaroniec, M. *J. Am. Chem. Soc.* **2006**, *128*, 14408–14414.
(13) Jin, Z.; Wang, X.; Cui, X. *Colloids Surf., A* **2008**, *316*, 27–36.
(14) Sayari, A.; Han, B.-H.; Yang, Y. *J. Am. Chem. Soc.* **2004**, *126*, 14348–14349.
(15) Kim, J. M.; Stucky, G. D. *Chem. Commun.* **2000**, 1159–1160.
(16) Ruthstein, S.; Frydman, V.; Kababya, S.; Landau, M.; Goldfarb, D. *J. Phys. Chem. B* **2003**, *107*, 1739–1748.
(17) Ruthstein, S.; Schmidt, J.; Kesselman, E.; Talmon, Y.; Goldfarb, D. *J. Am. Chem. Soc.* **2006**, *128*, 3366–3374.
(18) Flodstrom, K.; Wennerstrom, H.; Alfredsson, V. *Langmuir* **2004**, *20*, 680–688.
(19) Flodstrom, K.; Teixeira, C. V.; Amenitsch, H.; Alfredsson, V.; Linden, M. *Langmuir* **2004**, *20*, 4885–4891.
(20) Linton, P.; Alfredsson, V. *Chem. Mater.* **2008**, *20*, 2878–2880.
(21) Linton, P.; Rennie, A. R.; Zackrisson, M.; Alfredsson, V. *Langmuir* **2009**, *25*, 4685–4691.
(22) Khodakov, A. Y.; Zholobenko, V. L.; Imperor-Clerc, M.; Durand, D. *J. Phys. Chem. B* **2005**, *109*, 22780–22790.

(23) Zholobenko, V. L.; Khodakov, A. Y.; Imperor-Clerc, M.; Durand, D.; Grillo, I. *Adv. Colloid Interface Sci.* **2008**, *142*, 67–74.
(24) Sundblom, A.; Oliveira, C. L. P.; Pedersen, J. S.; Palmqvist, A. E. C. *J. Phys. Chem. C* **2010**, *114*, 3483–3492.
(25) Zhao, D.; Wan, Y. In *Introduction to Zeolite Science and Practice*, 3rd ed.; Cejka, J., Corma, H. v. B. A., Schütz, F., Ed.; Elsevier: Amsterdam, 2007; Vol. 168, pp 241−300.
(26) Kim, S. S.; Pauly, T. R.; Pinnavaia, T. J. *Chem. Commun.* **2000**, 1661–1662.
(27) Kim, S. S.; Karkamkar, A.; Pinnavaia, T. J.; Kruk, M.; Jaroniec, M. *J. Phys. Chem. B* **2001**, *105*, 7663–7670.
(28) Jammaer, J.; Aerts, A.; D'Haen, J.; Seo, J. W.; Martens, J. A. *J. Mater. Chem.* **2009**, *19*, 8290–8293.
(29) Martens, J. A.; Jammaer, J.; Bajpe, S.; Aerts, A.; Lorgouilloux, Y.; Kirschhock, C. E. A. *Microporous Mesoporous Mater.* **2011**, *140*, 2–8.
(30) Cundy, C. S.; Henty, M. S.; Plaisted, R. J. *Zeolites* **1995**, *15*, 353–372.
(31) Ju, J.; Zeng, C.; Zhang, L.; Xu, N. *Chem. Eng. J.* **2006**, *116*, 115–121.
(32) Zurner, A.; Kirstein, J.; Doblinger, M.; Brauchle, C.; Bein, T. *Nature* **2007**, *450*, 705–708.
(33) Chen, S. Y.; Tang, C. Y.; Chuang, W. T.; Lee, J. J.; Tsai, Y. L.; Chan, J. C. C.; Lin, C. Y.; Liu, Y. C.; Cheng, S. F. *Chem. Mater.* **2008**, *20*, 3906–3916.
(34) Lu, A. H.; Schuth, F. *Adv. Mater.* **2006**, *18*, 1793–1805.
(35) Huang, L.; Wind, S. J.; O'Brien, S. P. *Nano Lett.* **2003**, *3*, 299–303.
(36) Crowley, T. A.; Ziegler, K. J.; Lyons, D. M.; Erts, D.; Olin, H.; Morris, M. A.; Holmes, J. D. *Chem. Mater.* **2003**, *15*, 3518–3522.
(37) Eggenhuisen, T. M.; van Steenbergen, M. J.; Talsma, H.; de Jongh, P. E.; de Jong, K. P. *J. Phys. Chem. C* **2009**, *113*, 16785–16791.
(38) Linton, P.; Wennerstrom, H.; Alfredsson, V. *Phys. Chem. Chem. Phys.* **2010**, *12*, 3852–3858.
(39) Lee, H. I.; Kim, J. H.; Stucky, G. D.; Shi, Y. F.; Pak, C.; Kim, J. M. *J. Mater. Chem.* **2010**, *20*, 8483–8487.
(40) Livesey, A. K.; Brochon, J. C. *Biophys. J.* **1987**, *52*, 693–706.
(41) Koppel, D. E. *J. Chem. Phys.* **1972**, *57*, 4814–&.
(42) Sundblom, A.; Oliveira, C. L. P.; Palmqvist, A. E. C.; Pedersen, J. S. *J. Phys. Chem.* **2009**, *113*, 7706–7713.
(43) Alexandridis, P.; Holzwarth, J. F.; Hatton, T. A. *Macromolecules* **1994**, *27*, 2414–2425.
(44) Ganguly, R.; Aswal, V. K.; Hassan, P. A. *J. Colloid Interface Sci.* **2007**, *315*, 693–700.
(45) Ganguly, R.; Kumbhakar, M.; Aswal, V. K. *J. Phys. Chem. B* **2009**, *113*, 9441–9446.
(46) Denkova, A. G.; Mendes, E.; Coppens, M. O. *J. Phys. Chem. B* **2008**, *112*, 793–801.
(47) Denkova, A. G.; Mendes, E.; Coppens, M. O. *J. Phys. Chem. B* **2009**, *113*, 989–996.
(48) Kunz, W.; Henle, J.; Ninham, B. W. *Curr. Opin. Colloid Interface Sci.* **2004**, *9*, 19–37.
(49) Ablonczy, Z.; Lukács, A.; Papp, E. *Biophys. Chem.* **2003**, *104*, 249–258.
(50) Kline, S. R. *J. Appl. Crystallogr.* **2006**, *39*, 895–900.
(51) Chu, B.; Zhou, A.-K. In *Nonionic Surfactants: Polyoxyalkylene Block Copolymers*, 60th ed.; Nace, V. M., Ed.; Marcel Dekker: New York, 1996; Vol. 30, pp 67−136.
(52) Takahashi, R.; Nakanishi, K.; Soga, N. *J. Sol-Gel Sci. Technol.* **2000**, *17*, 7–18.
(53) Iler, R. *The Chemistry of Silica: Solubility, Polymerization, Colloid and Surface Properties and Biochemistry of Silica*; John Wiley & Sons: New York, 1979.
(54) Teixeira, C. V.; Amenitsch, H.; Linton, P.; Lindén, M.; Alfredsson, V. *Langmuir* **2011**, *27*, 7121–7131.
(55) Jammaer, J.; Aerts, A.; D'Haen, J.; Seo, J. W.; Martens, J. A. In *Stud. Surf. Sci. Catal.*; Gaigneaux, E. M., et al., Eds.; Elsevier: 2010; Vol. 175, pp 681−684.
(56) Gommes, C. J.; Friedrich, H.; Wolters, M.; Jongh, P. E. d.; Jong, K. P. d. *Chem. Mater.* **2009**, *21*, 1311–1317.
(57) Imperor-Clerc, M.; Manet, S.; Grillo, I.; Durand, D.; Khodakov, A.; Zholobenko, V. In *Zeolites and Related Materials: Trends, Targets and Challenges, Proceedings of the 4th International Feza Conference*; Gedeon, A., Massiani, P., Babonneau, F., Eds.; Elsevier Science Bv: Amsterdam, 2008; Vol. 174, pp 805−810.
(58) Ganguly, R.; Aswal, V. K.; Hassan, P. A.; Gopalakrishnan, I. K.; Yakhmi, J. V. *J. Phys. Chem. B* **2005**, *109*, 5653–5658.